ROYAL SOCIETY OF CHEMISTRY

EDGE ARTICLE

Check for updates

Stretchable electrode enabled electrochemical mass spectrometry for *in situ* and complementary analysis of cellular mechanotransduction†

Haotian Wang,[a] Jing Yan,[b] Jiamei Lin,[a] Caiying Zhang,[a] Xinglei Zhang,[a] Rui Su,*[c] Yan-Ling Liu*[b] and Jiaquan Xu ![ORCID] *[a]

Mechanotransduction exerts a profound influence on diverse cellular processes *via* activated signalling pathways. Although the currently established methods could reveal force-induced ultimate changes in specific biochemical cues, they fail to provide real-time and comprehensive information about the complicated signaling events. Herein, we report stretchable electrode enabled electrochemical mass spectrometry for *in situ* and complementary analysis of cellular mechanotransduction. The stretchable electrode functions as not only an electrochemical sensor for tracking the electroactive molecules released from stretched cells cultured thereon, but also an ionization source to ionize the intracellular metabolites for mass spectrometry analysis. As a concept application, the endothelial mechanotransduction mediated NO pathway was found to be different in transient stimulation and prolonged stimulation for the first time. This work provides a revealing strategy for *in situ* and comprehensive analysis of the biomolecules involved in cellular mechanotransduction.

Introduction

Mechanical forces play an integral role in living systems, operating at various levels ranging from the molecular to the cellular scale.[1,2] The sophisticated process by which cells sense and translate mechanical forces (*e.g.*, stretching tension, shear force, scratch and compression) into biochemical responses is known as cellular mechanotransduction.[3–5] Cellular mechanotransduction can be rapidly initiated (within a second) through mechanical deformation, and it subsequently triggers an intricate cascade reaction involving a myriad of molecules,[6] ranging from small molecules (*e.g.*, reactive oxygen species and nitrogen species) to genes, amino acids, aliphatic acids and proteins. Thus, to comprehensively understand the occurring mechano-transduction, it is crucial to develop a methodology that facilitates simultaneous *in situ* and real-time analysis of multiple molecules.

By now, a lot of methods have been applied for studying cellular mechanotransduction, including nuclear magnetic resonance (NMR),[7,8] fluorometry,[9–11] electrochemistry,[12,13] mass spectrometry (MS),[14,15] *etc.* Among them, electrochemical

sensing is widely accepted in detecting and quantifying transient release of biochemical molecules (*e.g.*, ROS, RNS) by living cells and tissues,[16–19] due to its rapid response time and exceptional sensitivity. Moreover, stretchable electrochemical sensors with high mechanical compliance enable *in situ* application of mechanical stimulation and real-time monitoring of biochemical molecules released from cells and tissues,[20–22] providing a unique tool to characterize the transient species related to mechanotransduction. However, most of the target analytes in electrochemical sensing are limited to electroactive molecules and the method has low throughput, thereby restricting the acquisition of multiple molecular information.[23–25] MS possesses the distinct advantage of simultaneous quantitative and qualitative analysis of multiple molecules with high sensitivity.[26–29] Particularly, ESI-MS and nanoESI-MS have frequently been employed to study mechanotransduction owing to their advantages in biomolecular analysis.[30–33] However, the requirement of complex sample pretreatment procedures prior to MS analysis has hindered their application in *in situ* studies of cellular mechanotransduction. In contrast, ambient ionization mass spectrometry (AIMS) enables the direct analysis of samples without or with minimal sample preparation, rendering it a powerful platform for real-time analysis of cellular mechanotransduction.[34–36] Nevertheless, the current ambient ionization source is inflexible and fails to accommodate cell deformation for *in situ* analysis of mechanotransduction,[37–39] and is not suitable for analysis of inorganic small molecules with short life (*e.g.*, ROS and RNS). Note that, the characteristics

[a]Jiangxi Key Laboratory for Mass Spectrometry and Instrumentation, East China University of Technology, Nanchang, 330013, P. R. China. E-mail: jiaquan_xu@foxmail.com

[b]Sauvage Center for Molecular Sciences, College of Chemistry and Molecular Sciences, Wuhan University, Wuhan 430072, P. R. China. E-mail: yanlingliu@whu.edu.cn

[c]State Key Laboratory of Inorganic Synthesis and Preparative Chemistry, Jilin University, Changchun, 130012, P. R. China. E-mail: rsu@jlu.edu.cn

of stretchable electrode electrochemistry and AIMS are complementary. Therefore, an integrated approach combining stretchable electrode electrochemistry and AIMS has the potential to provide real-time and comprehensive insights into the complex signaling events in cellular mechanotransduction. However, such a method has not yet been reported.

Recently, we introduced a simple approach to fabricate stretchable electrochemical biosensors by utilizing a conductive ink,[40] which was obtained by doping a small-molecule plasticizer (bis(trifluoromethane) sulfonimide lithium salt, LiTFSI) into poly(3,4-ethylenedioxythiophene):poly(styrene sulfonate) (PEDOT:PSS). Herein, inspired by the high processability, excellent stretchable property and prominent electrochemical stability of this conductive ink, we developed a convenient and highly controllable strategy to prepare stretchable electrode enabled electrochemical mass spectrometry (EC-MS) for *in situ* and complementary analysis of cellular mechanotransduction (Fig. 1). The stretchable electrode acted as both a stretchable electrochemical sensor and stretchable ionization source. According to the previous studies,[41] endothelial cells (ECs) represent a prototypical mechanosensitive cell type that responds to alterations in blood pressure and shear stress. In ECs, mechanical stimulation induces Piezo1-mediated Ca^{2+} influx. This cascade subsequently promotes the phosphorylation of AKT and nitric oxide synthase (NOS), leading to enhanced nitric oxide (NO) production and secretion. Thus, as a proof of concept of the present method, endothelial mechanotransduction was investigated in this work. The mechanotransduction of human umbilical vein endothelial cells (HUVECs) can be easily triggered by stretching the electrode. The electrochemical sensor effectively monitored the NO release, providing real-time and intuitive indication of mechanotransduction. In concert, *in situ* MS analysis provided metabolite variation in the mechanotransduction, using the stretchable electrode as an ambient ionization source.

Results and discussion

Mechanical and electrochemical properties of PPL/PDMS

As shown in Fig. 1a, the stretchable electrode PPL/PDMS was prepared by spin coating a mixture of poly(3,4-ethyldioxythiophene):poly(styrenesulfonate) and lithium bis(trifluoromethane)sulfonyl imide (PPL) onto a polydimethylsiloxane membrane (PDMS) according to the previous report.[40] Fig. S1† demonstrates that the stretchable electrode exhibits excellent transparency, which is beneficial for the microscopic characterization of cells on its surface. The stretchability of PPL/PDMS was systematically investigated. Fig. 2a illustrates the original PPL/PDMS, the stretched PPL/PDMS, and the bent PPL/PDMS. Scanning electron microscopy (SEM) was employed to characterize the structural variations in the PPL on PDMS after stretching. As illustrated in Fig. S2,† the electrode surface demonstrated negligible changes after 10% strain. Wrinkles started to emerge after 50% strain and became more prominent after 100% strain; however, no significant fissures were observed even at 100% strain, which was consistent with prior reports.[40] These results demonstrated that PPL/PDMS exhibited exceptional stretchability. To further investigate the electronic stability of PPL/PDMS, we meticulously monitored the fluctuation of resistance throughout the stretching process. The results shown in Fig. 2b indicated that the normalized resistance (R/R_0) exhibited negligibly small
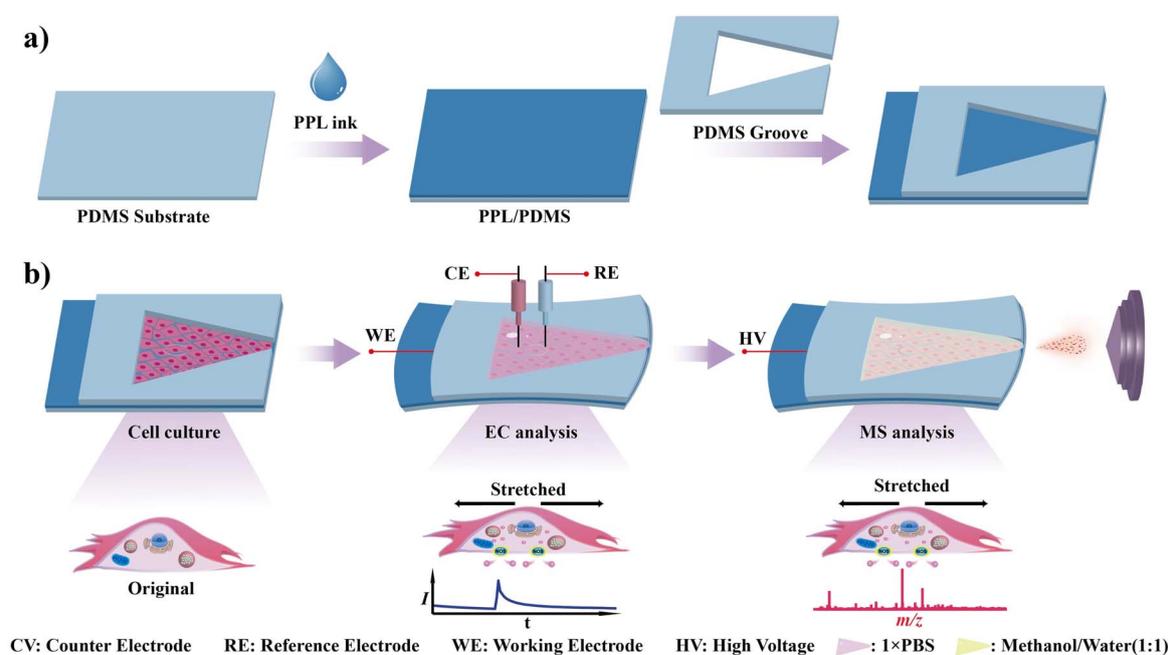

Fig. 1 Schematic illustration of the *in situ* analysis of cellular mechanotransduction by stretchable electrode enabled electrochemical mass spectrometry. (a) Preparation of the stretchable electrode; (b) *in situ* analysis of the cellular mechanotransduction by electrochemical mass spectrometry.
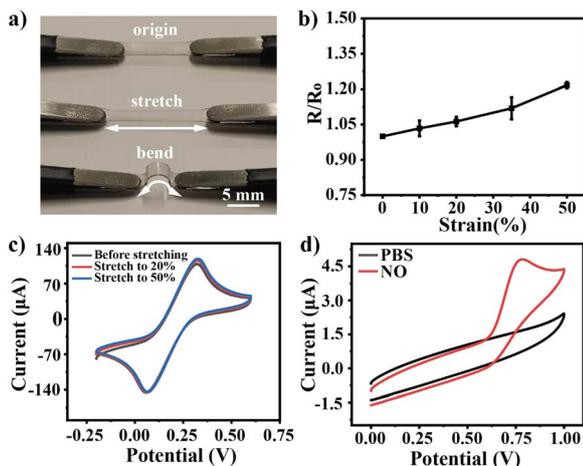
Fig. 2 Mechanical and electrochemical properties of PPL/PDMS. (a) Photographs of PPL/PDMS before and after deformation. (b) Resistance changes under 0–50% tensile strain ($n = 3$). "R" represents the resistance of the stretched electrode, whereas "R_0" denotes the resistance of the unstretched electrode. (c) CV curves of 10 mM $K_3[Fe(CN)_6]$ on PPL/PDMS at different tension states from 0 to 50%. (d) CV curves of the electrode in PBS buffer salt solution with and without 180 μM NO.

changes within a strain of up to 50%, thereby indicating the robustness of its electronic properties. The electrochemical stability of PPL/PDMS was further examined. Fig. 2c displays the cyclic voltammogram (CV) of $K_3[Fe(CN)_6]$ on PPL/PDMS under different deformations. The results showed that the shapes and peak current remained virtually unchanged when the electrode was subjected to strains of up to 50%, indicating that severe mechanical deformations had a negligible impact on the electrochemical properties. These results demonstrated that PPL/PDMS has good mechanical stretchability and electrochemical stability.

NO is an important signaling molecule of endothelial mechanotransduction.[42,43] Thus, the electrochemical sensing performance of the PPL/PDMS film for NO was investigated. As shown in Fig. 2d, an evident current peak at +0.75 V (vs. Ag/AgCl) was observed on PPL/PDMS in a 0.18 mM NO/PBS solution, while no discernible current response was detected on PPL/PDMS in a PBS buffer salt solution, thereby indicating the capability of PPL/PDMS to facilitate the oxidation of NO.[44–46] Moreover, as shown in Fig. S3,† the peak current and oxidation potential of NO on PPL/PDMS exhibited only slight variations after electrode stretching at 20% and 50%, further demonstrating the electrochemical stability of PPL/PDMS. Amperometric results displayed a good linear response to NO in a wide concentration range of 50 nM to 250 μM (Fig. S4†) on PPL/PDMS by applying +0.75 V, and even the response of 50 nM NO could be clearly observed. The detection limit was calculated to be approximately 10 nM (S/N = 3), showcasing the exceptional sensing capability of PPL/PDMS towards NO electrooxidation. The electrode's resistance to matrix interference was evaluated through electrochemical interference spiking experiments and cell lysate spiking recovery experiments. As depicted in Fig. S5,† the NO electrochemical response exhibited negligible variation

before and after the spiking of HUVEC lysate or potential interferents such as L-arginine, L-citrulline, L-aspartic acid, and ATP. This indicates that the PPL/PDMS electrode possesses excellent capability to resist matrix interference during NO detection. The biocompatibility of PPL/PDMS was also investigated. As shown in Fig. S6,† fusiform HUVECs exhibited significant proliferation after 36 hours of culture. Furthermore, Calcein-AM/PI staining revealed that the HUVECs exhibited robust vitality, thereby demonstrating the outstanding biocompatibility of PPL/PDMS. After detaching the HUVECs from the PPL/PDMS electrode, the electrochemical performance of the electrode was evaluated. As shown in Fig. S7,† the response to NO on the PPL/PDMS electrode showed only slight variations in both oxidation potential and oxidation current before and after HUVEC culture. These results demonstrate that PPL/PDMS possessed robust anti-fouling and repeatability properties. The remarkable capability of PPL/PDMS in detecting NO released from HUVECs was further demonstrated, the results are shown in Fig. S8.†

Characterization of the MS analytical performance of the stretchable ionization source

Subsequently, the ionization performance of PPL/PDMS was investigated. After applying +3 kV to 120% stretched PPL/PDMS (Fig. S9†), an obvious spray was formed at the tip of the film
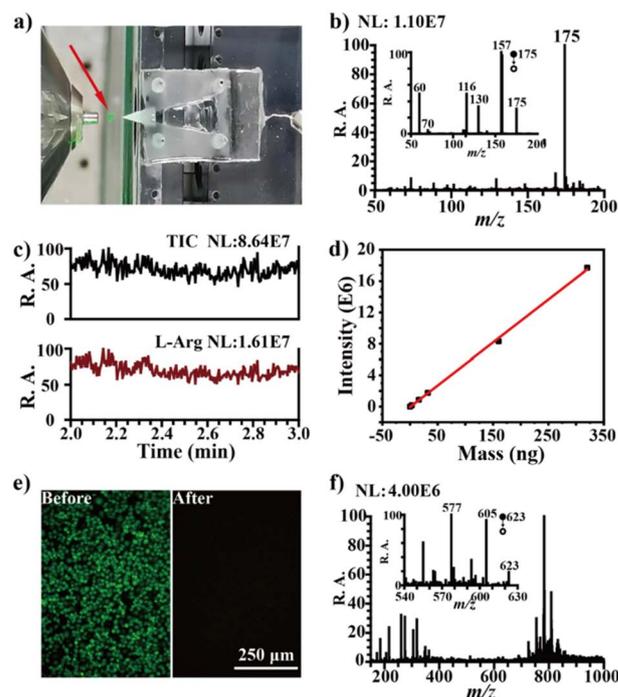

Fig. 3 Characterization of the MS analytical performance of the stretchable ionization source. (a) A photograph of the stretchable ionization MS. A stable plume was observed obviously marked by the red arrow. (b) Mass spectra of L-arginine. Inset is the MS/MS of m/z 175 [L-arginine + H]$^+$. (c) TIC and EIC of the L-arginine analysis. (d) The calibration curve of L-arginine. (e) Fluorescence microscopic images of Calcein-AM stained HUVECs on PPL/PDMS before and after applying + 3 kV using CH_3OH as the extraction solution. (f) MS/MS of m/z 623.

using CH_3OH as the extraction solution (Fig. 3a), which was attributed to the excellent conducting property ($R = 11.8\ \Omega/\square$). Fig. 3b displays the MS results of 10 ng L-arginine on PPL/PDMS, and an obvious signal at m/z 175 was observed, which can be assigned to [L-arginine + H]$^+$. The results were further confirmed by MS/MS shown in the inset of Fig. 3b, where m/z 157 was formed by the loss of H_2O from m/z 175, and m/z 158 was formed by the loss of NH_3 from m/z 175. As the angle of the conical electrospray tip significantly affects the spray performance, the influence of the spray tip angle on the MS signal was systematically investigated. As illustrated in Fig. S10,† an angle of 30° yields the strongest MS/MS signal of m/z 175 [L-arginine + H]$^+$, which is consistent with the previous reports.[47–49] The long-term stability and reproducibility were also investigated. As shown in Fig. S11 and S12,† the MS/MS signal showed almost no variation after two days, and the RSD of the stretchable ionization source was 5.7%, indicating that the present ionization was stable and reproducible. Moreover, the extracted ion chromatogram (EIC) of m/z 175 and total ion chromatogram (TIC) remained stable without significant attenuation during MS detection (Fig. 3c), indicating the robust and reliable ionization performance of PPL/PDMS. The sensitivity of this stretchable ionization MS was further investigated. Fig. 3d displays the standard curve of L-arginine obtained by stretchable ionization mass spectrometry, which shows a good linear relationship between the mass and the intensity of L-arginine in the range of 3 ng–300 ng. Based on the calibration curve, the LOD of the present method for L-arginine was calculated to be 1 ng according to LOD = $3\sigma/a$, where "σ" is the standard deviation of the blank and "a" is the slope of the calibration curve. These findings indicate that the stretchable ionization MS exhibits high sensitivity. The analytical performance of stretchable ionization MS for the analysis of molecules in HUVECs was subsequently investigated. Fig. 3e displays the fluorescence microscopic images of calcein-AM stained HUVECs before and after stretchable ionization MS analysis using CH_3OH as the extraction solution and +3 kV ionization voltage. The green fluorescence of HUVECs exhibited a remarkable reduction after MS analysis, implying the efficient extraction of fluorescent molecules from the HUVECs. MS/MS of the fluorescent molecule calcein ([M + H]$^+$, m/z 623) is shown in the inset of Fig. 3f, and characteristic fragment ions m/z 605 (–H_2O) and m/z 577 (–HCOOH) were observed, confirming that the fluorescent molecules were successfully extracted from HUVECs and ionized by a stretchable ionization source. These results demonstrated the applicability of the current stretchable ionization MS for metabolite analysis in HUVECs cultured thereon.

Real time monitoring of the endothelial mechanotransduction by electrochemical mass spectrometry

Subsequently, the endothelial mechanotransduction was investigated by stretchable electrode enabled electrochemical mass spectrometry. According to previous reports,[50–52] PPL/PDMS ionization with HUVECs cultured thereon was followed by a rapid 20% stretch within 1 s (marked as transient stimulation) to simulate hemangiectasis, resulting in approximately

10% deformation of the HUVECs (Fig. 4a). The results presented in Fig. 4a also demonstrate that the HUVECs adhered stably to the surface of the electrode during mechanical stimulation. This was further corroborated by the findings in Fig. S13,† which showed that no cells detached from the electrode surface after five cycles of electrode stretching. After the mechanical stimulation, the current rapidly increased to 80 μA within 1 s (Fig. 4b, red line), followed by a relatively slow decrease over approximately 30 seconds. In contrast, only a negligible mechanical disturbance was detected in the absence of cells under the same stimulation and detection conditions (Fig. 4b, black line). To confirm that the increased current was derived from NO release of HUVECs in response to the mechanical stimuli,[53,54] strain of 20% was applied after pretreating HUVECs with N^G-nitro-L-arginine methyl ester hydrochloride (L-NAME), a specific endothelial NOS (eNOS) inhibitor, and there was no signal produced (red line in Fig. 4b). These results demonstrated that the PPL/PDMS stretchable sensor could *in situ* induce and simultaneously monitor NO release derived from HUVEC mechanotransduction.

To delve deeper into the intricate biomolecular changes associated with endothelial mechanotransduction, we conducted *in situ* mass spectrometry analysis as soon as the currents rose. Fig. S14 and S15† display the mass spectra of the cells before and after 20% deformation ($n = 19$). More than 100 MS signals with S/N > 3 can be identified from the mass spectra. Then, the classic methods, principal component analysis (PCA) and orthogonal partial least squares–discriminant analysis (OPLS-DA) were applied to build classification models. As shown in Fig. 4c and S16a,† samples from the same group have a separation trend in the PCA score map, and the two groups of samples can be completely separated by the OPLS-DA score map. The non-targeted metabolomics profile can distinguish the control group and the mechanical stimulation group through the OPLS-DA model, which also shows that mechanical stimulation can lead to significant changes in molecules in HUVEC. A 200 permutation test was performed to validate the OPLS-DA model. As shown in Fig S16b,† the intersection point of the Q^2 regression line and the vertical axis is less than zero, suggesting that the model does not exhibit overfitting. Besides, the cumulative interpretation rate parameters R^2X and R^2Y of the OPLS-DA model are 0.887 and 0.91, respectively, and the predictive ability Q^2 parameter is 0.842, indicating that this model is stable and reliable.[55] With VIP (variable importance in the projection) > 1 and $P < 0.05$ as evaluation criteria, 18 biomarkers could be screened out. Tandem MS coupled with library search was further employed to identify the metabolites (Fig. S17†). The mass ion information for metabolites which were tentatively identified as potential biomarkers according to the Human Metabolome Database (HMDB) is summarized in Table S1,† including dihydrouracil, N-acetylputrescine, sulcatol, decanal, L-argininosuccinate, L-citrulline, dodecanoic acid, γ-linolenic acid, and L-arginine.

Fig. S18† displays the variation tendency of metabolites after mechanical stimulation. The upregulation of L-citrulline and the downregulation of L-arginine are closely correlated with NO release. This is consistent with previous findings, as L-arginine
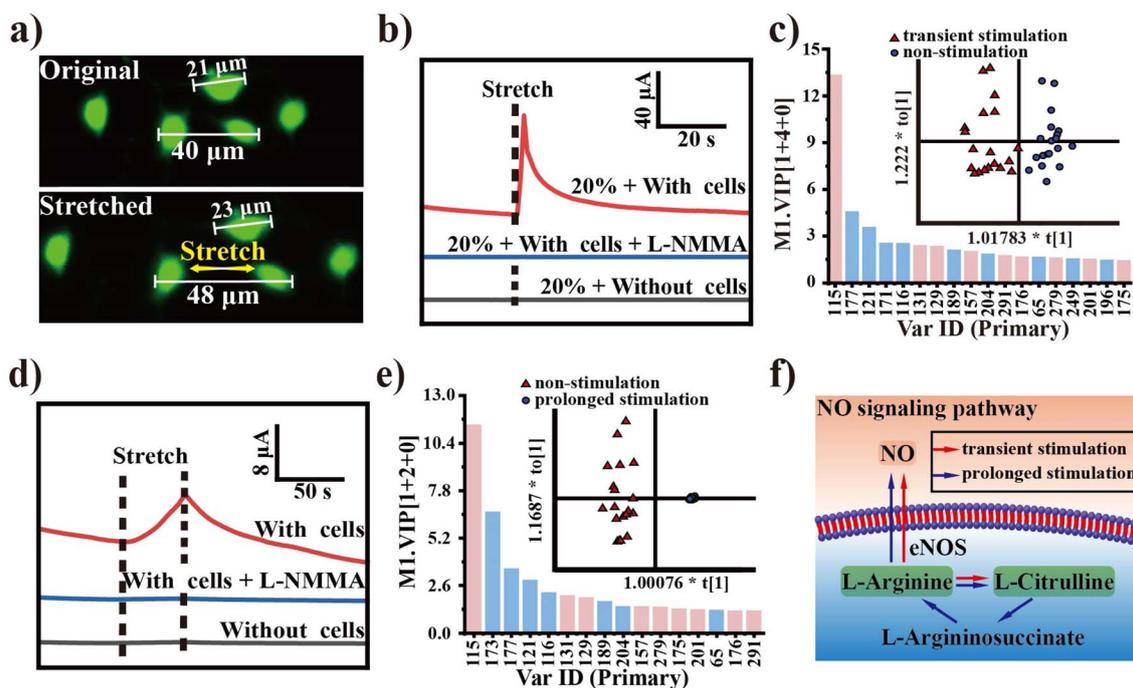
Fig. 4 Real time monitoring of the endothelial mechanotransduction by electrochemical mass spectrometry. (a) Fluorescence microscopic images of HUVECs cultured on PPL/PDMS stained with Calcein-AM before and after being stretched. (b) Current responses recorded from HUVECs submitted to 20% deformation with transient stimulation. (c) OPLS-DA score scatter plot and VIP bar plot of mass spectral data. (d) Current responses recorded from HUVECs submitted to 20% stimulation with prolonged stimulation. (e) OPLS-DA score scatter plot and VIP bar plot of mass spectral data. (f) Schematic diagram of NO related metabolic pathways during mechanotransduction.

serves as the substrate for NO production while L-citrulline is a by-product of this process.[56,57] This result demonstrated that the present method is feasible for analysis of the mechanotransduction. Besides, as a downstream product of L-arginine metabolism,[58–60] N-acetylputrescine was also downregulated alongside with L-arginine (Fig. S18†). L-argininosuccinate, a precursor of L-arginine, was administered to supplement L-arginine levels during mechanotransduction,[61] which also resulted in a notable reduction. According to previous reports,[62–64] upon mechanical stimulation of endothelial cells, prostacyclin, a remarkably potent vasodilator, would be significantly upregulated. Consequently, γ-linolenic acid, serving as a precursor for prostacyclin synthesis,[65–67] experiences increased consumption under such conditions, leading to a notable reduction in its cellular concentration (Fig. S18†). These results demonstrated that the present electrochemical mass spectrometry method is useful for in situ and complementary analysis of cellular mechanotransduction.

The velocity of vasodilation is disrupted in some cardiovascular diseases, such as myocarditis and atherosclerosis. Thus, to further investigate the impact of vasodilation velocity on mechanotransduction, we subjected HUVECs to a prolonged stretch stimulation, increasing deformation from 0% to 20% over a 60 second period. Consequently, the current increased slowly to 8 μA within 60 s (Fig. 4d, red line) and decreased slowly within about 100 s. Compared to the results shown in Fig. 4b, the results presented in Fig. 4d demonstrate a markedly prolonged NO release duration in prolonged stimulation. Similarly,

two control experiments were carried out and the results (blue line and black line in Fig. 4d) demonstrated that the increase in current was attributed to NO release.

The metabolites involved in the prolonged stimulation was also investigated by stretchable ionization MS. The mass spectra of the HUVECs after prolonged stimulation are shown in Fig. S19.† Then, PCA and OPLS-DA were empolyed to analyze the data present in Fig. S14 and S19.† As shown in Fig. 4e and S20a,† the same group samples were tightly clustered in both PCA and OPLS-DA score plot. The permutation test results (Fig. S20b†) indicated that the OPLS-DA model is not overfitting. The cumulative explanation rate parameters R^2X and R^2Y of the model are 0.613 and 0.972, respectively. The model's predictive ability Q^2 is 0.944, further indicating its stability and reliability. By using VIP > 1 and $P < 0.05$ as evaluation criteria, 16 biomarkers can be screened, which highly overlap with those in Fig. 4c. Fig. S21† illustrates the variation trend of metabolites after prolonged mechanical stimulation, which were all downregulated compared to non-stimulation. Moreover, in comparison to the metabolites depicted in Fig. S18,† those illustrated in Fig. S21† exhibited a further reduction. These results suggest that during prolonged stimulation, the associated metabolites were significantly depleted in response to the mechanical stimulation. Specifically, during prolonged stimulation, L-citrulline was downregulated (Fig. S21†), whereas under transient stimulation, L-citrulline is upregulated (Fig. S18†). These results indicated that the mechanotransduction mediated NO pathway is different in transient stimulation and prolonged stimulation.

Sequentially, a speculative mechanotransduction mediated NO pathway is presented in Fig. 4f. In transient stimulation, eNOS catalyzes L-arginine to produce NO and L-citrulline (red pathway in Fig. 4f), resulting in an increase in the NO and L-citrulline. In the prolonged duration of mechanical stimulation, eNOS first catalyzes L-arginine to produce NO and L-citrulline (red pathway in Fig. 4f), resulting in an increase in the NO and L-citrulline, which is the same as rapid stimulation. However, as the stimulation duration increased, L-arginine was progressively depleted, resulting in insufficient availability for NO production. To further respond to the mechanical stimulation, a compensation mechanism occurred to supplement L-arginine. According to a previous report,[68–70] a pathway to supplement L-arginine is proposed (blue pathway in Fig. 4f), where L-citrulline acts as a substrate to produce the L-arginine. The downregulation of L-argininosuccinate was further confirmed by this process (Fig. S21†).

Conclusions

In summary, we have developed a stretchable electrode enabled electrochemical mass spectrometry for *in situ* and complementary analysis of cellular mechanotransduction. The stretchable electrode acted as a stretchable electrochemical sensor and stretchable ionization source, which exhibited exceptional biocompatibility, electrical conductivity, ionization efficiency, and electrochemical performance. Inorganic small molecules (NO) and organic molecules (*e.g.*, L-citrulline, dodecanoic acid, γ-linolenic acid, and L-arginine, dihydrouracil, N-acetylputrescine) were detected in the Pt endothelial mechanotransduction. The mechanotransduction mediated NO pathway was found to be different in transient stimulation and prolonged stimulation for the first time. These results demonstrated that stretchable electrode enabled electrochemical mass spectrometry is a promising method for the *in situ* and comprehensive study of cellular mechanotransduction. In the future, we will further enhance the coverage of the present method in analysis of metabolites in cellular mechanotransduction by intergrating *in situ* electroporation, *in situ* enzymatic digestion, or other methods.

Data availability

The raw image data generated and analysed, that support the findings of this study, are available from the corresponding author upon reasonable request.

Author contributions

J. Q. Xu and Y.-L. Liu designed and supervised the research. H. T. Wang, J. Yan, J. M. Lin, and C. Y. Zhang conducted the experiments. Data analysis was performed by J. Q. Xu, Y.-L. Liu, R. Su, and X. L. Zhang. The manuscript was drafted by J. Q. Xu, Y.-L. Liu, and R. Su.

Conflicts of interest

The authors declare no competing interests.

References

1 B. Coste, J. Mathur, M. Schmidt, T. J. Earley, S. Ranade, M. J. Petrus, A. E. Dubin and A. Patapoutian, Piezo1 and Piezo2 are essential components of distinct mechanically activated cation channels, *Science*, 2010, **330**, 55–60.

2 N. W. Bellono, J. R. Bayrer, D. B. Leitch, J. Castro, C. Zhang, T. A. O'Donnell, S. M. Brierley, H. A. Ingraham and D. Julius, Enterochromaffin cells are gut chemosensors that couple to sensory neural pathways, *Cell*, 2017, **170**, 185–198.

3 N. Wang, J. D. Tytell and D. E. Ingber, Mechanotransduction at a distance: mechanically coupling the extracellular matrix with the nucleus, *Nat. Rev. Mol. Cell Biol.*, 2009, **10**, 75–82.

4 B. D. Hoffman, C. Grashoff and M. A. Schwartz, Dynamic molecular processes mediate cellular mechanotransduction, *Nature*, 2011, **475**, 316–323.

5 J. D. Humphrey, E. R. Dufresne and M. A. Schwartz, Mechanotransduction and extracellular matrix homeostasis, *Nat. Rev. Mol. Cell Biol.*, 2014, **15**, 802–812.

6 W. T. Fan, X. Qin, X. B. Hu, J. Yan, W. T. Wu, Y. L. Liu and W. H. Huang, Stretchable Electrode Based on Au@Pt Nanotube Networks for Real-Time Monitoring of ROS Signaling in Endothelial Mechanotransduction, *Anal. Chem.*, 2020, **92**, 15639–15646.

7 Y. Ito and P. Selenko, Cellular structural biology, *Curr. Opin. Struct. Biol.*, 2010, **20**, 640–648.

8 E. Luchinat and L. Banci, In-cell NMR: a topical review, *IUCrJ*, 2017, **4**, 108–118.

9 M. Alieva, A. K. Wezenaar, E. J. Wehrens and A. C. Rios, Bridging live-cell imaging and next-generation cancer treatment, *Nat. Rev. Cancer*, 2023, **23**, 731–745.

10 D. Entenberg, M. H. Oktay and J. S. Condeelis, Intravital imaging to study cancer progression and metastasis, *Nat. Rev. Cancer*, 2023, **23**, 25–42.

11 S. V. Venkateswaran, P. Kreuzaler, C. Maclachlan, G. McMahon, G. Greenidge, L. Collinson, J. Bunch and M. Yuneva, A multimodal imaging pipeline to decipher cell-specific metabolic functions and tissue microenvironment dynamics, *Nat. Protoc.*, 2025, **20**, 1678–1699.

12 J. Li, M. Su, M. Jiang, L. Tian, C. Zhu, X. Cao, Q. Jiang, X. Huo and C. Yu, Stretchable conductive film based on silver nanowires and carbon nanotubes for real-time inducing and monitoring of cell-released NO, *Sensor. Actuator. B Chem.*, 2022, **366**, 131983.

13 Y. Ling, Q. Lyu, Q. Zhai, B. Zhu, S. Gong, T. Zhang, J. Dyson and W. Cheng, Design of stretchable holey gold biosensing electrode for real-time cell monitoring, *ACS Sens.*, 2020, **5**, 3165–3171.

14 H. Zhang, K. H. Lu, M. Ebbini, P. Huang, H. Lu and L. Li, Mass spectrometry imaging for spatially resolved multi-omics molecular mapping, *Npj Imaging*, 2024, **2**, 20.

15 P. Romani, G. Benedetti, M. Cusan, M. Arboit, C. Cirillo, X. Wu, G. Rouni, V. Kostourou, M. Aragona and C. Giampietro, Mitochondrial mechanotransduction through MIEF1 coordinates the nuclear response to forces, *Nat. Cell Biol.*, 2024, **26**, 2046–2060.

16 W. T. Wu, X. Chen, Y. T. Jiao, W. T. Fan, Y. L. Liu and W. H. Huang, Versatile construction of biomimetic nanosensors for electrochemical monitoring of intracellular glutathione, *Angew. Chem., Int. Ed.*, 2022, **61**, e202115820.

17 Y.-T. Qi, H. Jiang, W.-T. Wu, F.-L. Zhang, S.-Y. Tian, W.-T. Fan, Y.-L. Liu, C. Amatore and W.-H. Huang, Homeostasis inside single activated phagolysosomes: quantitative and selective measurements of submillisecond dynamics of reactive oxygen and nitrogen species production with a nanoelectrochemical sensor, *J. Am. Chem. Soc.*, 2022, **144**, 9723–9733.

18 X.-K. Yang, F.-L. Zhang, X.-K. Jin, Y.-T. Jiao, X.-W. Zhang, Y.-L. Liu, C. Amatore and W.-H. Huang, Nanoelectrochemistry reveals how soluble Aβ42 oligomers alter vesicular storage and release of glutamate, *Proc. Natl. Acad. Sci.*, 2023, **120**, e2219994120.

19 Y. Yu, M. Pan, J. Peng, D. Hu, Y. Hao and Z. Qian, A review on recent advances in hydrogen peroxide electrochemical sensors for applications in cell detection, *Chin. Chem. Lett.*, 2022, **33**, 4133–4145.

20 X. Zhao, K. Wang, B. Li, C. Wang, Y. Ding, C. Li, L. Mao and Y. Lin, Fabrication of a flexible and stretchable nanostructured gold electrode using a facile ultraviolet-irradiation approach for the detection of nitric oxide released from cells, *Anal. Chem.*, 2018, **90**, 7158–7163.

21 M. Zhou, Y. Jiang, G. Wang, W. Wu, W. Chen, P. Yu, Y. Lin, J. Mao and L. Mao, Single-atom Ni-N4 provides a robust cellular NO sensor, *Nat. Commun.*, 2020, **11**, 3188.

22 Y. L. Liu and W. H. Huang, Stretchable Electrochemical Sensors for Cell and Tissue Detection, *Angew. Chem. Int. Ed.*, 2021, **60**, 2757–2767.

23 G. Ma, J. Zhou, C. Tian, D. Jiang, D. Fang and H. Chen, Luminol electrochemiluminescence for the analysis of active cholesterol at the plasma membrane in single mammalian cells, *Anal. Chem.*, 2013, **85**, 3912–3917.

24 A. Ramachandran, S. Panda and S. K. Yesodha, Physiological level and selective electrochemical sensing of dopamine by a solution processable graphene and its enhanced sensing property in general, *Sensor. Actuator. B Chem.*, 2018, **256**, 488–497.

25 Y. Yang, M. Li and Z. Zhu, A novel electrochemical sensor based on carbon nanotubes array for selective detection of dopamine or uric acid, *Talanta*, 2019, **201**, 295–300.

26 M. Zhao, X. Liu, Y. Hou, T. Yang, J. Xu and R. Su, Combination of electrochemistry and mass spectrometry to study nitric oxide metabolism and its modulation by compound K in breast cancer cells, *Anal. Chem.*, 2022, **94**, 5122–5131.

27 R. Yin, V. Prabhakaran and J. Laskin, Quantitative extraction and mass spectrometry analysis at a single-cell level, *Anal. Chem.*, 2018, **90**, 7937–7945.

28 R. M. Onjiko, S. A. Moody and P. Nemes, Single-cell mass spectrometry reveals small molecules that affect cell fates in the 16-cell embryo, *Proc. Natl. Acad. Sci. U. S. A.*, 2015, **112**, 6545–6550.

29 C. Lombard-Banek, S. A. Moody and P. Nemes, Single-Cell Mass Spectrometry for Discovery Proteomics: Quantifying Translational Cell Heterogeneity in the 16-Cell Frog (Xenopus) Embryo, *Angew Chem. Int. Ed. Engl.*, 2016, **55**, 2454–2458.

30 J. W. Frey, B. L. Jacobs, C. A. Goodman and T. A. Hornberger, A role for Raptor phosphorylation in the mechanical activation of mTOR signaling, *Cell. Signal.*, 2014, **26**, 313–322.

31 E. Crosas-Molist, V. Graziani, O. Maiques, P. Pandya, J. Monger, R. Samain, S. L. George, S. Malik, J. Salise and V. Morales, AMPK is a mechano-metabolic sensor linking cell adhesion and mitochondrial dynamics to Myosin-dependent cell migration, *Nat. Commun.*, 2023, **14**, 2740.

32 Y.-C. Yang, X.-D. Wang, K. Huang, L. Wang, Z.-L. Jiang and Y.-X. Qi, Temporal phosphoproteomics to investigate the mechanotransduction of vascular smooth muscle cells in response to cyclic stretch, *J. Biomech.*, 2014, **47**, 3622–3629.

33 S. Mao, W. Zhang, Q. Huang, M. Khan, H. Li, K. Uchiyama and J. M. Lin, In situ scatheless cell detachment reveals correlation between adhesion strength and viability at single-cell resolution, *Angew. Chem., Int. Ed.*, 2018, **57**, 236–240.

34 J. Wu, S. Wang, Q. Chen, H. Jiang, S. Liang and J.-M. Lin, Cell-patterned glass spray for direct drug assay using mass spectrometry, *Anal. Chim. Acta*, 2015, **892**, 132–139.

35 L. Song, K. Chingin, M. Wang, D. Zhong, H. Chen and J. Xu, Polarity-specific profiling of metabolites in single cells by probe electrophoresis mass spectrometry, *Anal. Chem.*, 2022, **94**, 4175–4182.

36 L. Zhang and A. Vertes, Single-cell mass spectrometry approaches to explore cellular heterogeneity, *Angew. Chem., Int. Ed.*, 2018, **57**, 4466–4477.

37 V. R. A. Filho and J. A. G. Neto, Evaluation of lubricating oil preparation procedures for the determination of Al, Ba, Mo, Si and V by high-resolution continuum source FAAS, *Anal. Sci.*, 2009, **25**, 95–100.

38 M. Jie, S. Mao, H. Li and J.-M. Lin, Multi-channel microfluidic chip-mass spectrometry platform for cell analysis, *Chin. Chem. Lett.*, 2017, **28**, 1625–1630.

39 R. Zenobi, Single-cell metabolomics: analytical and biological perspectives, *Science*, 2013, **342**, 1243259.

40 J. Yan, Y. Qin, W.-T. Fan, W.-T. Wu, S.-W. Lv, L.-P. Yan, Y.-L. Liu and W.-H. Huang, Plasticizer and catalyst co-functionalized PEDOT: PSS enables stretchable electrochemical sensing of living cells, *Chem. Sci.*, 2021, **12**, 14432–14440.

41 S. E. Murthy, A. E. Dubin and A. Patapoutian, Piezos thrive under pressure: mechanically activated ion channels in health and disease, *Nat. Rev. Mol. Cell Biol.*, 2017, **18**, 771–783.

42 Z. H. Jin, Y. L. Liu, W. T. Fan and W. H. Huang, Integrating flexible electrochemical sensor into microfluidic chip for

simulating and monitoring vascular mechanotransduction, *Small*, 2020, **16**, 1903204.

43 Y. Qin, X. B. Hu, W. T. Fan, J. Yan, S. B. Cheng, Y. L. Liu and W. H. Huang, A Stretchable Scaffold with Electrochemical Sensing for 3D Culture, Mechanical Loading, and Real-Time Monitoring of Cells, *Advanced Science*, 2021, **8**, 2003738.

44 Y. L. Liu, Z. H. Jin, Y. H. Liu, X. B. Hu, Y. Qin, J. Q. Xu, C. F. Fan and W. H. Huang, Stretchable electrochemical sensor for real-time monitoring of cells and tissues, *Angew. Chem., Int. Ed.*, 2016, **55**, 4537–4541.

45 Y. Wang, Y. Song, G. Zhu, D. Zhang and X. Liu, Highly biocompatible BSA-MnO$_2$ nanoparticles as an efficient near-infrared photothermal agent for cancer therapy, *Chin. Chem. Lett.*, 2018, **29**, 1685–1688.

46 J. Q. Xu, Y. L. Liu, Q. Wang, H. H. Duo, X. W. Zhang, Y. T. Li and W. H. Huang, Photocatalytically Renewable Micro-electrochemical Sensor for Real-Time Monitoring of Cells, *Angew. Chem., Int. Ed.*, 2015, **54**, 14402–14406.

47 T. M. H. Nguyen, W.-Y. Song and T.-Y. Kim, Characterization of spray modes and factors affecting the ionization efficiency of paper spray ionization, *Front. Chem.*, 2022, **10**, 864184.

48 J. Feng, Y. Yan, Y. Liu and J. Lengyel, A simple method for elemental analysis of liquids in sprayed microdroplets by laser-induced breakdown spectroscopy, *J. Anal. At. Spectrom.*, 2025, **40**, 114–121.

49 C. S. Jhang, H. Lee, Y. S. He, J. T. Liu and C. H. Lin, Rapid screening and determination of 4-chloroamphetamine in saliva by paper spray-mass spectrometry and capillary electrophoresis-mass spectrometry, *Electrophoresis*, 2012, **33**, 3073–3078.

50 B. Williams, Mechanical influences on vascular smooth muscle cell function, *J. Hypertens.*, 1998, **16**, 1921–1929.

51 C. Stefanadis, J. Dernellis, C. Vlachopoulos, C. Tsioufis, E. Tsiamis, K. Toutouzas, C. Pitsavos and P. Toutouzas, Aortic function in arterial hypertension determined by pressure-diameter relation: effects of diltiazem, *Circulation*, 1997, **96**, 1853–1858.

52 C. Stefanadis, C. Stratos, C. Vlachopoulos, S. Marakas, H. Boudoulas, I. Kallikazaros, E. Tsiamis, K. Toutouzas, L. Sioros and P. Toutouzas, Pressure-diameter relation of the human aorta: a new method of determination by the application of a special ultrasonic dimension catheter, *Circulation*, 1995, **92**, 2210–2219.

53 W.-T. Fan, Y. Zhao, W.-T. Wu, Y. Qin, J. Yan, Y.-L. Liu and W.-H. Huang, Redox homeostasis alteration in endothelial mechanotransduction monitored by dual stretchable electrochemical sensors, *Anal. Chem.*, 2022, **94**, 7425–7432.

54 Y.-W. Wang, Y.-L. Liu, J.-Q. Xu, Y. Qin and W.-H. Huang, Stretchable and photocatalytically renewable electrochemical sensor based on sandwich nanonetworks for real-time monitoring of cells, *Anal. Chem.*, 2018, **90**, 5977–5981.

55 Z.-H. Jin, Y.-L. Liu, J.-J. Chen, S.-L. Cai, J.-Q. Xu and W.-H. Huang, Conductive polymer-coated carbon nanotubes to construct stretchable and transparent electrochemical sensors, *Anal. Chem.*, 2017, **89**, 2032–2038.

56 C. Piras, M. Pibiri, S. Conte, G. Ferranti, V. P. Leoni, S. Liggi, M. Spada, S. Muntoni, P. Caboni and L. Atzori, Metabolomics analysis of plasma samples of patients with fibromyalgia and electromagnetic sensitivity using GC–MS technique, *Sci. Rep.*, 2022, **12**, 21923.

57 W. Li, X. Liu, H. Li, J. Zeng, Y. Chen and B. Xu, Metabolomic and transcriptomic insights into the mechanisms of renal ischemia-reperfusion injury progression, *Sci. Rep.*, 2024, **14**, 30101.

58 A. Figueroa, S. J. Jaime, M. Morita, J. U. Gonzales and C. Moinard, L-citrulline supports vascular and muscular benefits of exercise training in older adults, *Exerc. Sport Sci. Rev.*, 2020, **48**, 133–139.

59 A. M. Gonzalez and E. T. Trexler, Effects of citrulline supplementation on exercise performance in humans: A review of the current literature, *J. Strength Condit Res.*, 2020, **34**, 1480–1495.

60 A. Shatanawi, M. S. Momani, R. Al-Aqtash, M. H. Hamdan and M. N. Gharaibeh, L-Citrulline supplementation increases plasma nitric oxide levels and reduces arginase activity in patients with type 2 diabetes, *Front. Pharmacol.*, 2020, **11**, 584669.

61 M. J. Romero, D. H. Platt, R. B. Caldwell and R. W. Caldwell, Therapeutic Use of Citrulline in Cardiovascular Disease, *Cardiovasc. Drug Rev.*, 2006, **24**, 275–290.

62 R. Li, Y. Li, K. Jiang, L. Zhang, T. Li, A. Zhao, Z. Zhang, Y. Xia, K. Ge and Y. Chen, Lighting up arginine metabolism reveals its functional diversity in physiology and pathology, *Cell Metab.*, 2025, **37**, 291–304.

63 L. Zhou, W. Zhan and X. Wei, Clinical pharmacology and pharmacogenetics of prostaglandin analogues in glaucoma, *Front. Pharmacol*, 2022, **13**, 1015338.

64 R. A. Salazar-Gonzalez and D. W. Hein, Influence of N-acetyltransferase polymorphism in the N-acetylation of asparagine and putrescine, *Faseb. J.*, 2022, **36**, DOI: **10.1096/fasebj.2022.36.S1.R4723**.

65 U. N. Das, Essential fatty acids-a review, *Curr. Pharm. Biotechnol.*, 2006, **7**, 467–482.

66 X. Wang, H. Lin and Y. Gu, Multiple roles of dihomo-γ-linolenic acid against proliferation diseases, *Lipids Health Dis.*, 2012, **11**, 25.

67 P. Fischer, V. Bultel-Poncé, A. Guy, I. Gonzales, P. A. Conde, J. M. Galano, T. Durand and C. Oger, Straightforward Syntheses of Phytoprostanes and Dihomo-phytoprostanes-Non-enzymatic Metabolites of γ-Linolenic, Dihomo-γ-linolenic and Stearidonic Acids, *Eur. J. Org Chem.*, 2022, **2022**, e202200085.

68 A. Simon, L. Plies, A. Habermeier, U. Martiné and E. I. Closs, Role of Neutral Amino Acid Transport and Protein Breakdown for Substrate Supply of Nitric Oxide Synthase in Human Endothelial Cells, *Circ. Res.*, 2003, **93**, 813–820.

69 B. R. Flam, D. C. Eichler and L. P. Solomonson, Endothelial nitric oxide production is tightly coupled to the citrulline-NO cycle, *Nitric Oxide*, 2007, **17**, 115–121.

70 Z. Bahadoran, P. Mirmiran, K. Kashfi and A. Ghasemi, Endogenous flux of nitric oxide: Citrulline is preferred to Arginine, *Acta Physiol.*, 2021, **231**, e13572.